Available online at www.sciencedirect.com
ScienceDirect
Geochimica et Cosmochimica Acta 75 (2011) 469–482
Geochimica et Cosmochimica Acta
www.elsevier.com/locate/gca

Theoretical and experimental investigation of nickel isotopic fractionation in species relevant to modern and ancient oceans

Toshiyuki Fujii [a,*], Frédéric Moynier [b], Nicolas Dauphas [c], Minori Abe [d]

[a] Research Reactor Institute, Kyoto University, 2-1010 Asashiro Nishi, Kumatori, Sennan, Osaka 590-0494, Japan
[b] Department of Earth and Planetary Sciences and McDonnell Center for Space Sciences, Washington University in St. Louis, Campus Box 1169, 1 Brookings Drive, Saint Louis, MO 63130-4862, USA
[c] Origins Laboratory, Department of the Geophysical Sciences and Enrico Fermi Institute, The University of Chicago, 5734 South Ellis Avenue, Chicago, IL 60637, USA
[d] Department of Chemistry, Graduate School of Science and Engineering, Tokyo Metropolitan University, 1-1 Minami-Osawa, Hachioji-shi, Tokyo 192-0397, Japan

Received 6 July 2010; accepted in revised form 2 November 2010; available online 9 November 2010

Abstract

Nickel plays a central role as an enzyme co-factor in the metabolism of methanogenic Archaea. Methanogens can fractionate Ni isotopes during assimilation, opening the possibility of using the stable isotopic composition of Ni as a biomarker. However, other sources of Ni isotopic variations need to be evaluated before one can establish Ni isotopes as an unambiguous tracer of methanogenesis in the rock record. Equilibrium exchange of Ni between the different species present in the ocean is a potential source of isotopic fractionation. Through controlled laboratory experiments and theoretical calculations, we quantify equilibrium Ni isotope fractionation between different species relevant to the modern and ancient ocean: $Ni(H_2O)_6^{2+}$, $Ni(H_2O)_{18}^{2+}$, $NiOH(H_2O)_5^{+}$, $Ni(OH)_2(H_2O)_4$, $NiCl(H_2O)_5^{+}$, *cis*-$NiCl_2(H_2O)_4$, *trans*-$NiCl_2(H_2O)_4$, $NiHS(H_2O)_5^{+}$, $Ni(HS)_2(H_2O)_4$, $NiSO_4(H_2O)_4$, $NiHCO_3(H_2O)_4^{+}$, $NiCO_3(H_2O)_4$, and organic ligands (crown ether and oxalic acid). The magnitude of ligand-controlled Ni isotopic fractionation, approximately 1.25‰/amu (2.5‰ for the $^{60}Ni/^{58}Ni$ ratio), is similar to that previously measured in cultures of methanogenic Archaea.
© 2010 Elsevier Ltd. All rights reserved.

1. INTRODUCTION

Microbial activity can fractionate non-traditional stable isotopes, opening the possibility of using those variations to trace life in past geologic environments (e.g., Beard et al. 1999; Mandernack et al. 1999; Croal et al. 2004; Crosby et al. 2005; Balci et al. 2006; Cameron et al. 2009). However, abiotic processes can also impart measurable isotopic fractionations and should not be overlooked. Owing to its ubiquity in rocks and minerals, its complex redox chemistry, and its central role in biochemistry, Fe has received much attention in both experimental and theoretical studies (see Dauphas and Rouxel, 2006; Johnson et al., 2008, for some reviews).

Although Ni is less abundant than Zn, Cu or Fe in organisms, it plays a major role in some key enzymes such as the methyl-coenzyme M reductase found in methanogenic Archaea (Thauer, 1998), the Ni-containing superoxide dismutase that protects some photosynthetic organism from oxidative stress (Dupont et al., 2008), and it may be necessary for assimilation of nitrogen from urea in phytoplankton (Price and Morel, 1991). In the ocean, Ni shows a characteristic nutrient profile, however, its depletion in surface waters is not as drastic as it is for other metals (e.g., Sclater et al., 1976; Bruland, 1980; Bruland and Lohan, 2003).

* Corresponding author. Tel.: +81 724 51 2469; fax: +81 724 51 2634.
E-mail address: tosiyuki@rri.kyoto-u.ac.jp (T. Fujii).

0016-7037/$ - see front matter © 2010 Elsevier Ltd. All rights reserved.
doi:10.1016/j.gca.2010.11.003

It has been speculated that Ni could have played a central role in controlling the evolution of redox conditions at Earth's surface. Konhauser et al. (2009) measured a decrease in the Ni concentration of banded iron formations at 2.7 Gyr ago, associated with a decrease in the occurrence of ultramafic magmatism. They argued that such decrease might have triggered the "Great Oxidation Event" on Earth. With less Ni, methanogens could not have released as much methane and, through a cascade of events, this would have contributed to a major increase in the oxygen level in the atmosphere.

Cameron et al. (2009) showed that Ni isotopes could be fractionated by methanogenic Archaea, which preferentially assimilate light Ni isotopes while the residual growth medium in all experiments and in the cell biomass from the non-methanogenic control organism (*P. calidifontis*) shows essentially no isotopic fractionation. The fractionation of up to 1.46‰ for $^{60}Ni/^{58}Ni$ ratio (~0.73‰/amu) in methanogens is much larger than any effect measured in extraterrestrial samples, terrestrial basalts, or continental sediments (e.g., 0.15 ± 0.24‰; Cook et al., 2007; Moynier et al., 2007; Cameron et al., 2009). While this first foray into Ni isotope biogeochemistry is encouraging, other sources of Ni isotopic variations need to be evaluated before one can use Ni isotopes as unambiguous tracers of methanogenesis in ancient rocks.

For example, exchange of Ni between the different species present in the ocean represents a potential source of isotopic fractionation. Nickel is distributed in the modern ocean between inorganic species (e.g., Ni^{2+}, $NiCl^{+}$, $NiCl_2$, $NiCO_3$, $NiHCO_3^{+}$, and $NiSO_4$) and some organic ligands (denoted L) of unspecified nature (Turner et al., 1981; Byrne et al., 1988; Donat et al., 1994; Saito et al., 2004; Turner and Martino, 2006; Vraspir and Butler, 2009). Turner et al. (1981) calculated the speciation of dissolved Ni in seawater in the absence of organic ligand and found the following proportions, Ni^{2+} (47%), $NiCl^{+}$ and $NiCl_2$ (34%), $NiCO_3$ and $NiHCO_3^{+}$ (14%). In presence of an organic ligand, NiL can dominate (e.g., Turner and Martino, 2006). It is worth noting that in the ancient ocean, the speciation could have been different and it is unknown if organic ligands were present. Thermodynamic calculations for Proterozoic and Archean oceans, give $NiHS^{+}$ as the dominant species under certain conditions (Saito et al., 2003).

In this study, we have investigated both theoretically and experimentally the isotopic fractionation of Ni between some of the major species present in the modern and ancient oceans: $Ni(H_2O)_6^{2+}$, $Ni(H_2O)_{18}^{2+}$, $NiOH(H_2O)_5^{+}$, $Ni(OH)_2(H_2O)_4$, $NiCl(H_2O)_5^{+}$, *cis*-$NiCl_2(H_2O)_4$, *trans*-$NiCl_2(H_2O)_4$, $NiHS(H_2O)_5^{+}$, $Ni(HS)_2(H_2O)_4$, $NiSO_4(H_2O)_4$, $NiHCO_3(H_2O)_4^{+}$, and $NiCO_3(H_2O)_4$.

It is difficult to assess the degree of Ni isotopic fractionation associated with organic ligands found in natural systems. As a first order approach, we performed equilibration experiments with a synthetic ligand (a crown ether, dicyclohexano-18-crown-6, DC18C6) and performed computations for Ni complexation with oxalic acid ($C_2H_2O_4$).

The equilibrium isotopic fractionations were calculated for the different Ni complexes present in solution by using the reduced partition function ratio (RPFR or β factors) of the different isotopologues (Urey, 1947; Bigeleisen and Mayer, 1947). The RPFR of the hydrated Ni ion, chloride, hydrogen sulfide, and oxalate can be calculated from thermodynamic data and structural data (Frisch et al., 2003), which is not the case of Ni coordinated with the crown ether (Ni–DC18C6). The RPFR of the Ni–DC18C6 complex are estimated from the isotopic fractionation factor obtained in an isotopic exchange experiment. Two sets of experiments at different HCl concentrations (4.7 and 8.5 mol/L, M) were performed to test the effect of speciation on Ni isotopic fractionation.

2. METHODS

2.1. Computational methods

Orbital geometries, vibrational frequencies, Gibbs free energies of aqueous Ni(II) species were computed using density functional theory (DFT) as implemented by the Gaussian 03 code (Frisch et al., 2003). The DFT method employed here is a hybrid density functional consisting of Becke's three-parameter non-local hybrid exchange potential (B3) (Becke, 1993) with Lee–Yang and Parr (LYP) (Lee et al., 1988) non-local functionals. The 6-311+G(d,p) basis set, which is an all-electron basis set, was chosen for H, C, O, S, Cl, and Ni. For the solvation effect, CPCM continuum solvation method (CPCM: conductor-like polarizable continuum model) was used.

The contribution of the nuclear volume was estimated by using the numerical multiconfigurational Dirac–Coulomb Hartree–Fock (MCDCHF) method, which was implemented in the four-component relativistic atomic program package GRASP2K (Jönsson et al., 2007). The electronic structures of Ni^0 ($[Ar]3d^84s^2$) and Ni^{2+} ($[Ar]3d^8$) were calculated. Vibrational, solvent, dynamic correlation, magnetic Breit interaction, and quantum electrodynamics effects were neglected. The Fermi statistical distribution function was adopted as a finite nucleus model. Root mean square radii reported in the literature (Fricke and Heilig, 2004) were used in the calculation. The default values in GRASP2K were adopted for the other conditions or parameters (Jönsson et al., 2007; Abe et al., 2008a).

2.2. Extraction experiments and isotopic analyses

Dicyclohexano-18-crown-6 (DC18C6) (over 97% purity) was a product of Fluka Chemie GmbH. Nickel dichloride (hydrated, 99.95% purity) was a product of Sigma–Aldrich, Co., Inc. Hydrochloric acid, in which the Ni impurity was certified to be less than 2.2 ppt, was purchased from Kanto Chemical, Co., Inc. Other chemicals were reagent grade from Wako Pure Chemical Industries, Ltd.

Nickel dichloride was dissolved in HCl to make solutions ranging from 0.8 to 1.8 M Ni(II) in 3.8–8.5 M HCl. The organic phase was diluted in chloroform to make a solution of 0.2 M DC18C6. A 1 mL aqueous solution and a 10 mL organic solution were mixed in a glass vial with a magnetic stirrer, and the glass vial was sealed. The proportion of the two phases was chosen based on the reported

low extractability of Ni(II) by DC18C6 (Nishizawa et al., 1997). The two phases were stirred for 30 min using a Teflon-coated magnetic bar. Equilibrium for crown ether systems is usually achieved within 30–60 s (Jepson and Cairns, 1979; Nishizawa et al., 1984). After equilibrium was attained, the two phases were separated by centrifugation at 2000 rpm for 1 min. An 8 mL aliquot of the organic solution was pipetted for back extraction. Nickel that had partitioned in DC18C6 was stripped into 8 mL of pure water. These steps were carried out at ~285 K. The Ni concentration in the back extraction water was analyzed by inductively coupled plasma atomic emission spectrometry (Shimadzu, ICPS-100TR).

Purification of back-extracted Ni was carried out to minimize potential isobaric interferences with Ni isotopes, notably from ^{58}Fe at mass 58 and from organic compounds. Samples in 1 mL of 1 M HCl were loaded on Bio-Rad polypropylene columns filled with 2 mL of cation-exchange resin (AG50-X8, 100–200 mesh) previously cleaned with 6 M HCl then conditioned with 10 mL 1 M HCl. The matrix was removed with 5 mL of 1 M HCl. Finally, Ni was eluted with 10 mL 6 M HCl and the eluate was evaporated to dryness. The yields were over 98%.

The solutions of purified Ni (5 ppm in 0.3 M HNO_3) were analyzed on a Neptune (Thermo Scientific) multi-collector inductively coupled plasma mass spectrometer (MC-ICPMS) at the Origins Laboratory of the University of Chicago (Dauphas et al., 2008). Aluminum cones were used. Isotopes ^{58}Ni, ^{60}Ni, ^{61}Ni, and ^{62}Ni were analyzed on Faraday collectors connected to $10^{11}\,\Omega$ amplifier. Because of the small abundance of ^{64}Ni (0.9%), this isotope is challenging to analyze by MC-ICPMS (Dauphas et al., 2008) and is not discussed here. Potential isobaric interference from $^{58}Fe^{+}$ on $^{58}Ni^{+}$ was corrected by monitoring $^{57}Fe^{+}$ ion beam intensity. High resolution mode was used to resolve interferences from $^{40}Ar^{16}O^{1}H^{+}$ and $^{40}Ar^{18}O^{+}$ at masses 57 and 58. Zoom optics were used to accommodate the mass dispersion (mass 57–66) in the collector array. On-peak zero intensities from blank solutions were subtracted from all measurements. The reference material used for sample-standard bracketing was SRM-986 (Gramlich et al., 1989). Each sample solution was analyzed 5 or 6 times by standard-sample bracketing.

In order to assess the accuracy of the isotopic measurements, an extraction procedure by DC18C6 was performed without Ni. The back extraction water was then purified as previously described. Following purification, a portion of the starting Ni material was added to this fraction and the Ni isotopic composition of this solution was analyzed. The determined isotopic composition was identical to that of the starting material within analytical error. Using these values, the experimental bias was estimated to be <0.08‰/amu.

3. RESULTS AND DISCUSSION

3.1. Isotope fractionation of Ni in solvent extraction

The species of Ni(II) in HCl medium in the laboratory experiment are Ni^{2+}, $NiCl^{+}$, and $NiCl_2$, which are related through the following stepwise reactions,

$$Ni^{2+} + Cl^{-} \rightleftarrows NiCl^{+} \quad (1)$$

$$NiCl^{+} + Cl^{-} \rightleftarrows NiCl_2 \quad (2)$$

Fig. 1 shows the mole fractions of Ni species estimated by using the apparent stability constants K_1 and K_2 of reactions 1 and 2 (Bjerrum, 1988). The formation of the nickel chloride species is possible in conditions of elevated acidity.

The extraction reaction of Ni(II) with the macrocyclic ligand may be written as,

$$NiCl_2 + L \rightleftarrows NiLCl_2 \quad (3)$$

where L stands for DC18C6. The distribution ratio D is written with moralities as,

$$D = \frac{\sum[\mathrm{Ni(II)}]_{org}}{\sum[\mathrm{Ni(II)}]_{aq}} \approx \frac{[NiLCl_2]}{[Ni^{2+}] + [NiCl^{+}] + [NiCl_2]} \quad (4)$$

where subscripts org and aq stand for the organic and aqueous phases, respectively. D is rewritten with apparent stability constants K_1 (reaction 1), K_2 (reaction 2), and K_{ex} (reaction 3) as,

$$D = \frac{K_1 K_2 K_{ex}[Cl^{-}]^2[L]}{1 + K_1[Cl^{-}] + K_1 K_2[Cl^{-}]^2} \quad (5)$$

Measured D values are shown in Fig. 2 as a function of HCl molarity. The D values are smaller than 10^{-4} and show an increase with acidity. The fitted D values based on Eq. (5) are shown together as a dotted curve. The results can be fitted with $K_{ex} = 0.00084$. Small misfit between calculated and experimental data (Fig. 2) may be due to the lack of precise activity coefficients of Ni(II) species in highly concentrated HCl solutions.

The isotope separation factor α_m, between the aqueous and the organic phases, is defined as:

$$\alpha_m = \frac{(\sum[^m\mathrm{Ni}]/\sum[^{58}\mathrm{Ni}])_{org}}{(\sum[^m\mathrm{Ni}]/\sum[^{58}\mathrm{Ni}])_{aq}} \quad (6)$$

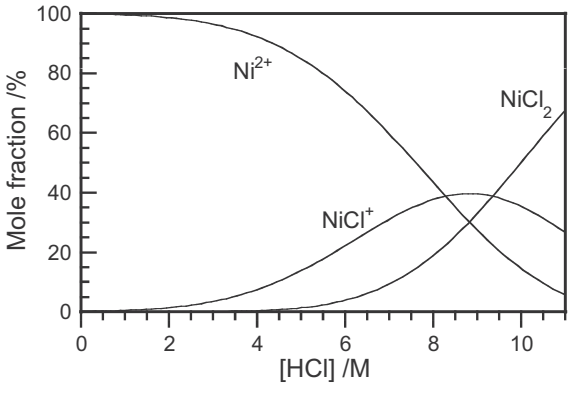

Fig. 1. Ni chlorides in HCl solutions. Distribution of Ni chlorides. The mole fractions were calculated from the reported stability constants (Bjerrum, 1988). The mean activity coefficient of HCl was used for the activity coefficient of Cl^{-}. The activity coefficient at any acidity was estimated by interpolation between published values (Bjerrum, 1988), in which K_1 is reported to be 0.01 for reaction 1. Since the reported stability constant of reaction 2 (K_2) ranges between 0.003 and 0.008, an intermediate value of $K_2 = 0.0055$ was used.

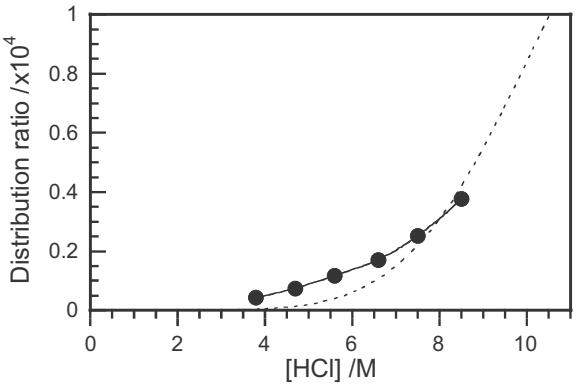

Fig. 2. Distribution ratios in $NiCl_2$–DC18C6 system. The dotted curve was calculated using reported K_1 and K_2 (reactions 1 and 2, respectively) (Bjerrum, 1988) and K_{ex} (=0.00084) determined in the present study. Following Bjerrum (1988), the activity of Cl^- ($\gamma[Cl^-]$) was used as $[Cl^-]$.

where the superscript m indicates the mass of a particular isotope ($m = 60$, 61 or 62). $(\Sigma[^m\text{Ni}]/\Sigma[^{58}\text{Ni}])_{org}$ and $(\Sigma[^m\text{Ni}]/\Sigma[^{58}\text{Ni}])_{aq}$ are the isotopic ratios of $^m\text{Ni}/^{58}\text{Ni}$ measured in the organic and aqueous phases, respectively, summed over all the species present in each phase. Because of the very small value of D (Fig. 2), most Ni stays in the aqueous phase and the $^m\text{Ni}/^{58}\text{Ni}$ ratio of the starting material (hydrated $NiCl_2$) can be substituted for $(\Sigma[^m\text{Ni}]/\Sigma[^{58}\text{Ni}])_{aq}$. For example, with $D = 10^{-4}$ and $\alpha_m = 1.001$ a shift of $\sim 0.0001‰$ for the $^m\text{Ni}/^{58}\text{Ni}$ ratio of the aqueous phase relative to the starting material would be expected. The isotope enrichment factor is defined as $\alpha_m - 1$. Because $\alpha_m \approx 1$, $\alpha_m - 1 \approx \ln \alpha_m$. In the present paper, we use the δ notation,

$$\delta^m\text{Ni} = \left(\frac{([^m\text{Ni}]/[^{58}\text{Ni}])_{\text{species/phase}}}{([^m\text{Ni}]/[^{58}\text{Ni}])_{\text{initial}}} - 1\right) \times 1000 \quad (7)$$

Because the Ni isotopic composition of the aqueous phase remains almost unchanged, δ^mNi of the organic phase is similar to $10^3 \ln \alpha_m$. It should be noted that in studies on Ni isotope fractionation in natural systems, δ^mNi is referenced to a standard like SRM-986. In the present study, δ^mNi corresponds to the difference in Ni isotopic composition between the organic phase and the starting material (aqueous phase). The δ^mNi values obtained are shown in Table 1. At both acidities (3.8 and 8.5 M), the organic phase is enriched in the lighter isotopes.

The classic theory of chemical isotope fractionation is based on mass-dependent isotopic differences in vibrational energies of isotopologues (Urey, 1947; Bigeleisen and Mayer, 1947). The isotope enrichment factor is proportional to $\delta m/mm'$, where $\delta m = m - m'$ with m and m' the masses of two isotopes (prime represents the light isotope). The conventional theory of mass-dependent fractionation was expanded by Bigeleisen (1996) to take into account the nuclear field shift effect,

$$\ln \alpha = \frac{hc}{kT} v_{fs} a + \frac{1}{24}\left(\frac{h}{2\pi kT}\right)^2 \frac{\delta m}{mm'} b \quad (8)$$

where v_{fs} is the nuclear field shift, a the nuclear field shift scaling factor, b the scaling factor for the conventional mass-dependent effect, h the Plank constant, c the light velocity, k the Boltzmann constant, and T the temperature. The nuclear field shift effect was identified as the cause of the mass-independent isotope fractionation in chemical exchange reactions (Bigeleisen, 1996; Nomura et al., 1996; Fujii et al., 2009a). The nuclear field shift results from differences in nuclear size and shape of different isotopes (Fricke and Heilig, 2004; King, 1984). Different isotopes have the same number of protons, but they do not have the same distribution of protons in space. The nuclear charge distribution, which is usually represented as the mean-square charge radius $<r^2>$, is affected by the number of neutrons in the nucleus. The nuclear charge distribution produces an electric field, and its variation from one isotope to another shifts the atomic energy levels, also displacing the electronic molecular states. The nuclear field shift is not mass-dependent but is strongly related to the neutron configuration of the nucleus.

The nuclear field shift is proportional to the isotopic difference in the mean-square charge radius, $\delta<r^2>$ (King, 1984). $<r^2>$ of ^{m}Ni increases with mass number, but the relationship, $\delta<r^2>$ *vs.* $\delta m/mm'$ does not follow a simple straight line (Fricke and Heilig, 2004). In order to identify a possible relationship between δ^mNi and $\delta<r^2>$, the mass dependent component was removed by using the exponential law of mass fractionation (Albarède et al., 2004; Russell et al. 1977, 1978). This normalization is effective for revealing the mass-independent component of the isotopic variations (Fujii et al., 2009b,c, 2010). The results of the equilibration experiments with DC18C6 are displayed in Fig. 3. Plots of δ^mNi *vs.* $\delta m/mm'$ (Fig. 3b and c) show similar profiles to $\delta<r^2>$ *vs.* $\delta m/mm'$ (Fig. 3a). However, considering the large uncertainties in Fig. 3b and c, we cannot resolve the presence of a nuclear field shift effect in Ni isotopes.

Recent quantum chemical studies have adopted finite nucleus models into *ab initio* methods (Schauble, 2007; Abe et al., 2008a,b, 2010). Nuclear field shift effects have been documented for Hg, Tl, and U redox reactions. Since the electron density at the nucleus is larger for *s*-orbital, the presence or absence of *s*-electrons may cause a larger

Table 1
Isotopic fractionation of nickel during exchange experiments between HCl medium and a macrocyclic complex (see text for details). Ni bound to the organic ligand is systematically lighter than Ni dissolved in HCl.

[HCl]/M	δ^{60}Ni	δ^{61}Ni	δ^{62}Ni	δ^{64}Ni
4.7	-1.72 ± 0.08	-2.40 ± 0.17	-3.37 ± 0.16	-1.9 ± 2.4
8.5	-1.50 ± 0.10	-2.17 ± 0.26	-2.96 ± 0.21	-7.2 ± 1.1

Errors are 2σ.

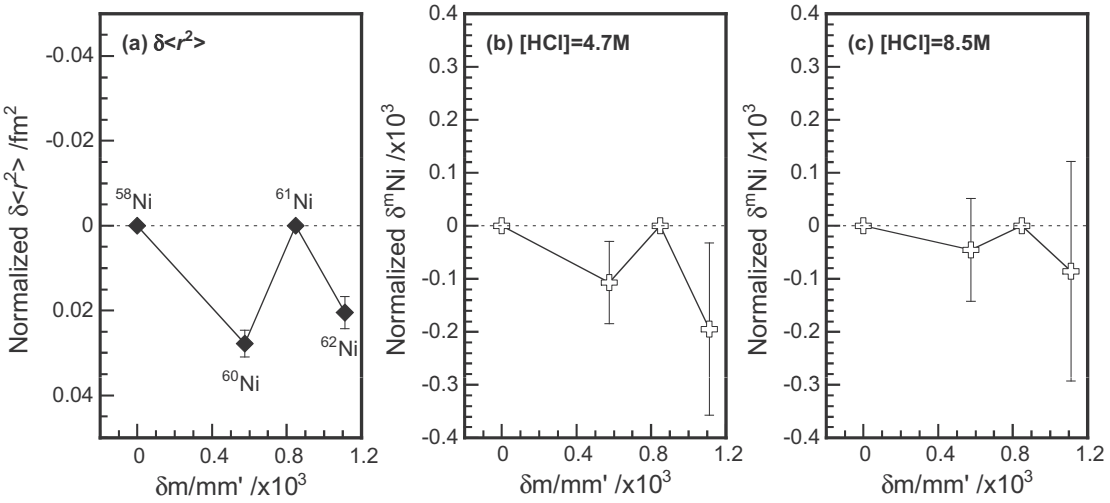

Fig. 3. Normalized δ^mNi and $\delta\langle r^2\rangle$ as functions of $\delta m/mm'$. δ^mNi values and relative $\delta\langle r^2\rangle$values (Fricke and Heilig, 2004) are normalized to the isotope pair ^{61}Ni/^{58}Ni by using the exponential law (Albarède et al., 2004). Errors are the same as those shown in Table 1. (a) Normalized $\delta\langle r^2\rangle$. (b) Normalized δ^mNi values for the [HCl] = 4.7 M experiment. (c) Normalized δ^mNi for the [HCl] = 8.5 M experiment.

Table 2
Total energy of Ni(II) and Ni^0 isotopes and calculated nuclear field shift effect for the Ni^0–Ni^{2+} exchange reaction.

Mass number	$\langle r^2\rangle^{1/2}$/fm	Ni^{2+} total energy/a.u.	Ni^0 total energy/a.u.	Nuclear field shift effect[a]/x10^{-3}
58	3.776	−1518.51221333	−1519.36507200	0.000
60	3.813	−1518.51209952	−1519.36495812	−0.076
61	3.823	−1518.51206858	−1519.36492716	−0.096
62	3.842	−1518.51200958	−1519.36486813	−0.136
64	3.860	−1518.51195343	−1519.36481194	−0.173

[a] The nuclear field shift effect is calculated by $\ln K_{fs} = \{\delta E(Ni^0) - \delta E(Ni^{2+})\}/kT$ at $T = 285$ K. Energy of photons of 1 a.u. is equal to 2.1947×10^5 cm^{-1} or 4.3597×10^{-18} J.

nuclear field shift effect. In the present study, the total electronic energies at the ground states of Ni^0 [(Ar)3$d^8$4s^2] and Ni^{2+} [(Ar)3d^8] were calculated for different isotopes with different nuclear charge radii. The root mean square radii ($\langle r^2\rangle^{1/2}$) reported in the literature (Fricke and Heilig, 2004) were used in the calculation. The results of those calculations are shown in Table 2 in atomic units (a.u.). As an example, the nuclear field shift effect in the Ni^0–Ni^{2+} redox reaction was estimated (Table 2). The estimated magnitude is much smaller than experimentally documented Ni isotopic fractionation in aqueous systems (Cameron et al., 2009; this study). This suggests that the isotopic fractionation of Ni originates from mass differences rather than a nuclear field shift effect.

3.2. β-Factors of Ni species

The isotope enrichment factor due to the intramolecular vibrations can be evaluated from the RPFR (Bigeleisen and Mayer, 1947), $(s/s')f$,

$$\ln(s/s')f = \sum[\ln b(u_i') - \ln b(u_i)] \quad (9)$$

where

$$\ln b(u_i) = -\ln u_i + u_i/2 + \ln(1 - e^{-ui}) \quad (10)$$

and

$$u_i = h\nu_i/kT \quad (11)$$

and ν stands for vibrational frequency. The subscript i stands for the ith molecular vibrational level with primed variables referring to the light isotopologue. The isotope enrichment factor due to the molecular vibration can be evaluated from the frequencies (ν) summed over all the different modes. $(s/s')f$ is equivalent to the β notation commonly encountered in geochemistry.

3.2.1. Nickel ion

Extensive structural studies of $Ni(H_2O)_6^{2+}$ have been carried out (Caminiti et al., 1977; Neilson and Enderby, 1978; Sandstrom, 1979; Magini, 1981; Magini et al., 1982; Waizumi et al., 1992a,b, 1999). In order to evaluate the strength of mass-dependent effects, quantum chemical calculations of the vibrational energies of the hydrated Ni(II) species were performed. Because of the excellent convergence of the reaction energies of Ni(II) species, using a basis set higher than 6-311+G(d,p) is recommended (Rulíšek and Havlas, 1999). For our quantum chemical calculations, we therefore selected the basis set 6-311+G(d,p). The hydrated Ni(II) species is generally thought to be present as octahedral $Ni(H_2O)_6^{2+}$. The calculated bond length of Ni–O and the literature values are reported in Table 3. The Ni–O bond length obtained is identical to the value determined with the same basis set (Rulíšek and Havlas, 1999), and the value agrees with experimental data (Caminiti et al., 1977;

Table 3
Bond length determined for $Ni(H_2O)_6^{2+}$.

Method[a]	Bond, Ni–O/Å	Reference
DFT	2.086	This work
DFT[b]	2.073 (4.464)[c]	This work
DFT	2.002	Waizumi et al. (1992b)
DFT	2.087	Rulíšek and Havlas (1999)
XRD	2.05–2.06	Caminiti et al. (1977)
XRD[d]	2.069	Magini (1981)
XRD[d]	2.056–2.072	Magini et al. (1982)
ND[e]	2.07–2.10	Neilson and Enderby (1978)
EXAFS	2.07	Sandstrom (1979)

[a] DFT (density functional theory), XRD (X-ray diffraction), ND (neutron diffraction), EXAFS (extended X-ray absorption fine structure).
[b] 12 H_2O were arranged in the second hydration sphere.
[c] Ni–O bond length for hydration waters in the second hydration sphere is shown in parentheses.
[d] Solutions contain $Ni(H_2O)_{6-n}Cl_n^{2-n}$ ($n = 0$, 1, and 2).
[e] D_2O was used.

Neilson and Enderby, 1978; Sandstrom, 1979; Magini, 1981; Magini et al., 1982). In some *ab initio* electronic structure studies, 12 H_2O molecules are set to the second hydration sphere (Bock et al., 2006; Rudolph and Pye, 1999). We also performed structural analysis of a larger cluster $Ni(H_2O)_{18}^{2+}$. The calculated bond lengths of Ni–O are shown in Table 3. Taking into account the second hydration sphere resulted in shortening the Ni–O bond length by only 0.013 Å in the first coordination sphere.

The intramolecular vibrational frequency analysis was then performed for aqueous Ni(II) species with optimized geometries. The calculation results for the symmetric vibrational frequency ν_1 are also shown in Table 4. The ν_1 frequencies determined by Raman spectrometry (Edwards and Knowles, 1992; Bickley et al., 1993) are shown together for comparison. The calculated ν_1 frequency of $Ni(H_2O)_6^{2+}$ is smaller than the values obtained experimentally. This is due to the fact that the calculation does not adequately treat the effect of solvation. When the second hydration sphere is taken into account as $Ni(H_2O)_{18}^{2+}$, the calculated ν_1 frequency agrees with the experimentally determined values (Pye et al., 2006).

The hydration enthalpy of $Ni(H_2O)_n^{2+}$ ($n = 6$ or 18) was also examined. In order to relate the calculated quantities to the experimental hydration enthalpy ($\Delta H°_{hyd}$) at 298 K, the following correction terms were considered (Li et al., 1996),

$$-\Delta H°_{hyd} = -\Delta E_b + \Delta E_{sol} + n\Delta H_{vap} + \Delta nRT - \Delta E(Cp) - \Delta E_{zp} + \Delta E_{rel} + \Delta E_{geom} \quad (12)$$

ΔE_b is the total binding energy of the gas phase cluster $[Ni(H_2O)_n]$. ΔE_{sol} represents the solvation free energy of $Ni(H_2O)_n^{2+}$. This term, which contains the entropic contribution to the solvation free energy for the continuum dielectric part, was neglected. ΔH_{vap} is the heat of vaporization of water, which is 10.50 kcal/mol (Lide, 2008). The $\Delta E(Cp)$ term arises from the difference in heat capacity of the components of the system, which corresponds to a small correction of ~1 kcal/mol at 298 K (Li et al., 1996). ΔE_{zp} is the difference in vibrational zero-point energy in forming clusters, ΔE_{rel} is a correction due to relativistic effects for metal centers, and ΔE_{geom} is a correction due to geometry relaxation for H_2O during the formation of the clusters. The last three terms tend to cancel out (a few kcal/mol) (Li et al., 1996), and these corrections were not included in our calculation. The calculated value of $\Delta H°_{hyd}$ is shown in Table 5. The hydration enthalpy of metal cations has been determined by thermochemical methods (Rosseinsky, 1965; Smith, 1977; Marcus, 1985), and literature values are shown for comparison. The $\Delta H°_{hyd}$ value obtained agrees well with a value reported by Rosseinsky (1965). Li et al. (1996) showed that, for divalent cations, even small cluster models like $Ni(H_2O)_6^{2+}$ can reproduce $\Delta H°_{hyd}$.

Based on the validity of the calculation of $Ni(H_2O)_6^{2+}$, ln β was determined by using Eqs. (9)–(11). The ln β values

Table 4
Totally symmetric vibrational frequencies of Ni(II) aqua-complexes.

Hydration number n	Method	Frequency (cm^{-1})	Reference
6	DFT	347	This work
18	DFT	394	This work
–	Raman[a]	390	Edwards and Knowles (1992)
–	Raman[b]	395	Bickley et al. (1993)

[a] Sample was a solution of Ni(II) formate.
[b] Sample was a solution of Ni(II) malonate.

Table 5
Hydration enthalpy of $Ni(H_2O)_n^{2+}$.

Hydration number n	$\Delta H°_{hyd}$/kcal/mol	Reference
6	515	This work
18	538	This work
–	518	Rosseinsky (1965)
–	503	Smith (1977)
–	502	Marcus (1985)

Table 6
Logarithm of the reduced partition function, ln β, for isotope pair $^{60}Ni/^{58}Ni$.

Species	ln β at 285 K/‰	ln β at 298 K/‰
$Ni(H_2O)_6^{2+}$	5.909	5.432
$Ni(H_2O)_{18}^{2+}$	6.576	6.046
$NiOH(H_2O)_5^{+}$	6.209	5.715
$Ni(OH)_2(H_2O)_4$	6.044	5.569
$NiCl(H_2O)_5^{+}$	5.771	5.305
cis-$NiCl_2(H_2O)_4$	5.250	4.825
trans-$NiCl_2(H_2O)_4$	5.213	4.787
$NiHS(H_2O)_5^{+}$	5.175	4.756
$Ni(HS)_2(H_2O)_4$	4.782	4.395
$NiSO_4(H_2O)_5$	6.242	5.877
$NiHCO_3(H_2O)_4^{+}$	6.295	5.787
$NiCO_3(H_2O)_4$	6.508	5.989
Ni–crown complex	4.177	3.859[a]
NiC_2O_4	6.900	6.348
$Ni(C_2O_4)_2^{2-}$	6.392	5.872
$Ni(C_2O_4)_3^{4-}$	4.660	4.275

[a] Estimated as ln $\beta = 4.177 \times \left(\frac{285}{298}\right)^2$.

at 285 and 298 K for the isotope pair ^{58}Ni–^{60}Ni are shown in Table 6. The temperature dependence of ln β is shown in Fig. 4 in the temperature range of 273–423 K (0–150 °C). The variation of ln β within this temperature range is ~4‰. The ln β value of hydrated Ni^{2+} using only the first coordination sphere was 5.432‰ (298 K), while setting the second hydration sphere increased ln β by *ca.* 1‰ (6.046‰ at 298 K). It should be noted that, in studies on Fe isotope fractionation, some difficulties to reproduce experimental data from theoretical calculations have been reported (Anbar et al., 2005; Domagal-Goldman et al., 2008; Hill et al., 2009). It is of interest that, for trivalent cations like Fe^{3+}, a larger cluster model including second coordination shell brings calculation data closer to the experimental results (Li et al., 1996). Using the larger cluster model including second coordination sphere or more may shift the theoretical estimate closer to the experimental result.

3.2.2. Nickel hydroxide

The structure of the first Ni hydrolysis product $NiOH(H_2O)_5^+$ was calculated using a cluster model (Li et al., 1996). That of the second hydrolysis product $Ni(OH)_2(H_2O)_4$ was calculated as a point symmetry (*trans*-type) based on the structure of $NiOH(H_2O)_5^+$. The calculated Ni–O bond lengths for $NiOH(H_2O)_5^+$ are 1.944 Å (Ni–OH) and 2.11–2.14 Å (Ni–H_2O), while those for $Ni(OH)_2(H_2O)_4$ are 1.998 Å (Ni–OH) and 2.17–2.19 Å (Ni–H_2O). The Ni–O bond length for the hydroxyl ion is shorter than that for hydrated water due to its stronger electron affinity to Ni^{2+}. Hydrolysis seems to loosen the hydration bond as shown by the Ni–O (H_2O) bond lengths reported in Table 3. The ln β values (at 298 K) were calculated to be 5.715‰ for $NiOH(H_2O)_5^+$ and 5.569‰ for $Ni(OH)_2(H_2O)_4$. According to Eqs. (9)–(11), one might expect that the stronger Ni–O (OH) bond should increase ln β, but the weaker Ni–O (H_2O) bond actually decreases it (Table 6).

3.2.3. Nickel chloride

The structure of $NiCl(H_2O)_5^+$ was calculated. The bond lengths converged to values of 2.11–2.13 Å (Ni–O) and 2.29 Å (Ni–Cl) (Table 7), but unfortunately structural data of pure $NiCl(H_2O)_5^+$ is not available for comparison. The structure of $NiCl_2(H_2O)_4$ can be in *cis*- and *trans*-geometries (Mizuno, 1961; Kleinberg, 1969; Agulló-Rueda et al., 1987; Waizumi et al., 1992b; Ptasiewicz-Bak et al., 1999). Structural studies on $NiCl_2(H_2O)_4$ crystals indicated that *cis*-$NiCl_2(H_2O)_4$ was the dominant species (Waizumi et al., 1992b; Ptasiewicz-Bak et al., 1999), while other studies found that *trans*-$NiCl_2(H_2O)_4$ was dominant (Mizuno, 1961; Kleinberg, 1969; Agulló-Rueda et al., 1987). Therefore, the geometries of both *cis*- and *trans*-$NiCl_2(H_2O)_4$ species were calculated. The bond lengths of the optimized structures are shown in Table 7. Though the result of our calculation for the Ni–O bond length of *cis*-$NiCl_2(H_2O)_4$ is slightly longer compared to literature data, the other Ni–O and Ni–Cl bond lengths are acceptable. The Gibbs free energies at 298 K were also calculated. The calculation was performed with and without solvation (hydration). The results are shown in Table 8. Without solvation, *cis*-$NiCl_2(H_2O)_4$ is more stable than *trans*-$NiCl_2(H_2O)_4$, while *trans*-$NiCl_2(H_2O)_4$ is more stable than *cis*-$NiCl_2(H_2O)_4$ if solvation is included.

The ln β values at 285 and 298 K are shown in Table 6. The ln β values of *cis*- and *trans*-$NiCl_2(H_2O)_4$ species are similar (4.825‰ and 4.787‰ at 298 K, respectively), which suggests that the structural details of $NiCl_2(H_2O)$ species do not have a large influence on the Ni isotopic fractionation. The nickel chloride relevant to the ocean chemistry may be $NiCl^+$ with ln $\beta = 5.305$‰ at 298 K.

3.2.4. Nickel sulfide

According to the reported stability constants (Saito et al., 2003; Al-Farawati and van den Berg, 1999), the formation of nickel sulfide species is possible in conditions of

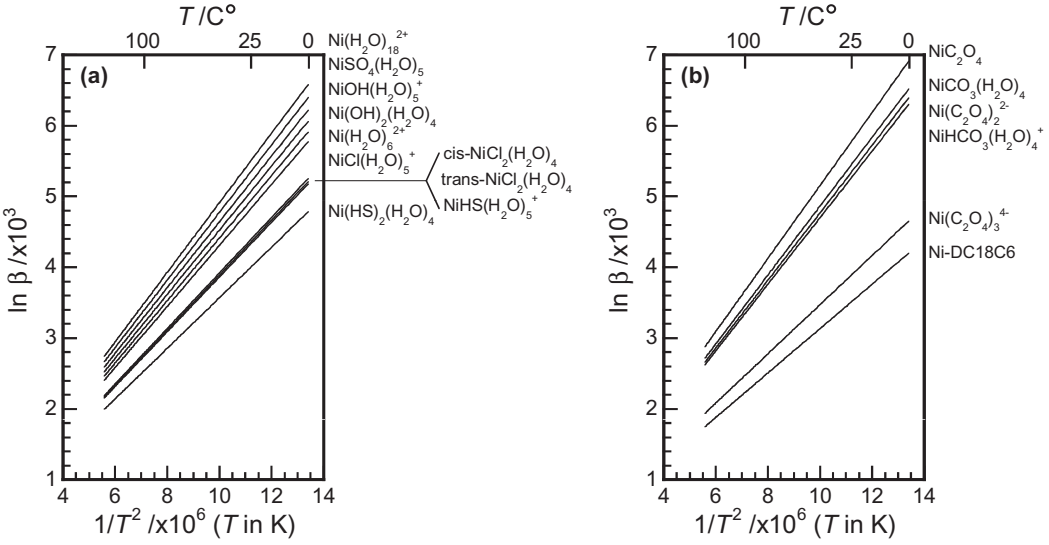

Fig. 4. Temperature dependence of ln β. Using ln β values at 298 K (Table 6), ln $\beta\,(T) = \ln\beta\,(298) \times (298/T)^2$ was calculated. The calculated ln $\beta\,(T)$ values are shown as functions of $1/T^2$. (a) Inorganic species (b) organic species and carbonates.

Table 7
Bond lengths determined for $NiCl(H_2O)_5^+$ and $NiCl_2(H_2O)_4$.

Species	Method[a]	Bond, Ni–O/Å	Bond, Ni–Cl/Å	Reference
$NiCl(H_2O)_5^+$	DFT	2.11–2.13	2.289	This work
cis-$NiCl_2(H_2O)_4$	DFT	2.14–2.16	2.358	This work
cis-$NiCl_2(H_2O)_4$	XRD	2.058–2.080	2.374–2.397	Waizumi et al. (1992b)
cis-$NiCl_2(H_2O)_4$	XRD	2.053–2.081	2.371–2.395	Ptasiewicz-Bak et al. (1999)
trans-$NiCl_2(H_2O)_4$	DFT	2.108–2.109	2.347	This work
trans-$NiCl_2(H_2O)_4$	XRD	2.10	2.38	Mizuno (1961)
trans-$NiCl_2(H_2O)_4$	ND	2.05	2.359	Kleinberg (1969)
–[a]	XRD	2.069	2.44	Magini (1981)
–[a]	XRD	2.056–2.072	2.431–2.468	Magini et al. (1982)
–[a]	XRD	2.05–2.07	2.36–2.37	Waizumi et al. (1999)

[a] Solutions contain $Ni(H_2O)_{6-n}Cl_n^{2-n}$ ($n = 0$, 1, and 2).

Table 8
Gibbs free energy of $NiCl_2(H_2O)_4$ at 298 K.

Species	Solvation	$G°$/hartree	$G°$/kcal/mol	$\Delta G°$/kcal/mol
cis	None	−2734.709375	−1716057.48	−1.91
trans	None	−2734.706336	−1716055.57	
cis	CPCM	−2734.765972	−1716093.00	3.12
trans	CPCM	−2734.770948	−1716096.12	

CPCM: conductor-like polarizable continuum model.

elevated $[HS^-] > 10^{-7}$ M. Six-coordination transition metal sulfides are considered to possess similar structures to that of $MnHS(H_2O)_5^+$ and $Mn(HS)_2(H_2O)_4$ (Rickard and Luther, 2006), in which $Mn(HS)_2$ is *trans*-$Mn(HS)_2(H_2O)_4$. According to the recommended structures, nickel hydrogen sulfides, $NiHS(H_2O)_5^+$ and $Ni(HS)_2(H_2O)_4$ were computed. The calculated bond lengths for $NiHS(H_2O)_5^+$ were 2.329 Å (Ni–S) and 2.13–2.15 Å (Ni–O), while those for $Ni(HS)_2(H_2O)_4$ were 2.41–2.42 Å (Ni–S) and 2.17–2.18 Å (Ni–O). The ln β values obtained for Ni sulfides are reported in Table 6. The ln β values (298 K) for $NiHS(H_2O)_5^+$ and $Ni(HS)_2(H_2O)_4$ were calculated to be 4.756‰ and 4.395‰, respectively. The ln β values of sulfides are ~0.5‰ smaller than those of chlorides. The Ni–ligand bond distances of Ni sulfides are longer than those of Ni chlorides (see Table 7). This suggests that the weaker interactions between Ni^{2+} and ligands in sulfides compared to chlorides resulted in smaller ln β for the former.

3.2.5. Nickel sulfate

The crystal structures of anhydrous and hydrous $NiSO_4$ have been studied by XRD (X-ray diffraction) (Dimaras, 1957; Ptasiewicz-Bak et al., 1997), ND (neutron diffraction) (O'Connor and Dale, 1966), and EXAFS (extended X-ray absorption fine structure) (Pattanaik et al., 2007) analyses. The structural studies on hydrous $NiSO_4$ crystals show the presence of 6 hydrated water molecules in an octahedral arrangement in the first coordination sphere of Ni^{2+}. No direct ion paring of Ni^{2+} and SO_4^{2-} is observed. The ion paring between Ni^{2+} and SO_4^{2-} in sulfate solutions has been studied by NMR (nuclear magnetic resonance) (Bechtold et al., 1978) and XRD (Licheri at al., 1982, 1986; Caminiti, 1982, 1986) analyses. The exchange rate of H_2O and SO_4^{2-} in the first coordination sphere of Ni^{2+} was studied by NMR (Bechtold et al., 1978), which demonstrated the existence of $NiSO_4(H_2O)_5$ and $NiSO_4(H_2O)_4$ in sulfate solutions. At 298 K, $NiSO_4(H_2O)_5$ is predominant compared to $NiSO_4(H_2O)_4$ (Bechtold et al., 1978). The calculated structure of $NiSO_4(H_2O)_5$ agreed with a structural model proposed by Magini (1979) (see model b′ reported on $FeSO_4(H_2O)_5^+$). The calculated bond lengths as well as the literature data are reported in Table 9. The calculated ln β value at 298 K is 5.877‰ (Table 6), which is 1.1–1.5‰ larger than those of Ni sulfides.

3.2.6. Nickel carbonate

Chemical behavior of Ni aqueous carbonates is less known (Hummel and Curti, 2003; Baeyens et al., 2003, and references therein). To our knowledge, structural data of monomers of $NiHCO_3^+$ and $NiCO_3$ in aqueous solutions are not available. There are several crystallographic studies on polynuclear Ni complexes in metallocarbonate systems (for example, Wikstrom et al., 2010, and references therein), in which CO_3^{2-} acts as monodentate and/or bidentate ligands to Ni complexes. Here, we treated CO_3^{2-} as the bidentate ligand to Ni^{2+} and computed $NiHCO_3^+$ as $NiHCO_3(H_2O)_4^+$ according to a core structure of Ni carbonate complexes (see "coordination mode *d*" of Fig. 2 by Escuer et al., 1996). The structure of $NiCO_3$ was also computed as $NiCO_3(H_2O)_4$, in which H^+ is dissociated from $NiHCO_3(H_2O)_4^+$. The ln β values of nickel carbonate complexes are compiled in Table 6. The ln β values (298 K) for $NiHCO_3(H_2O)_4^+$ and $NiCO_3(H_2O)_4$ were calculated to be 5.787‰ and 5.989‰, respectively. These are larger than those of Ni chlorides and sulfides, and are similar to that of sulfate.

Table 9
Bond lengths determined for Ni sulfates.

Species or media	Method	Bond, Ni–O/Å	Bond, Ni–S/Å	Bond, S–O/Å	Angle, Ni–S–O/°	Reference
$NiSO_4(H_2O)_5$	DFT	2.06–2.08[a]	3.07	1.45–1.59	118	This work
1 M $NiSO_4$ + 2.88 M H_2SO_4	XRD	2.126	–	1.51[b]	–	Caminiti (1982)
2 M $NiSO_4$	XRD	2.063	–	1.50[b]	–	Caminiti (1982)
2 M $NiSO_4$	XRD	2.068	3.49	1.50[b]	–	Licheri et al. (1984)
2 M $NiSO_4$	XRD	2.070	–	1.51[b]	–	Licheri et al. (1984)
2 M $NiSO_4$	XRD	2.059	–	1.49[b]	–	Caminiti (1986)
1.5 M $NiSO_4$ + 3.0 M Li_2SO_4	XRD	2.059	–	1.51[b]	–	Caminiti (1986)
–[c]	–[c]	2.06[c]	3.2–3.35[c]	1.49[c]	130–140[c]	Caminiti (1986)
$NiSO_4$	XRD	1.99	3.13[d]	1.53	125[d]	Dimaras (1957)
$NiSO_4$	XRD	2.06	3.20[d]	1.60	121[d]	Dimaras (1957)
$NiSO_4{\cdot}6H_2O$	ND	2.02–2.10	–	1.48–1.46	–	O'connor and Dale (1966)
$NiSO_4{\cdot}7H_2O$	XRD	2.031–2.078	–	1.464–1.471	–	Ptasiewicz-Bak et al. (1997)
$NiSO_4{\cdot}nH_2O$	EXAFS	2.05	–	–	–	Pattanaik et al. (2007)

[a] Ni–O bond length for the nearest O atom of SO_4^{2-} in the first coordination sphere of Ni was converged to be 1.99 Å.
[b] Calculated from O–O distance of SO_4^{2-} as it is the regular tetrahedron.
[c] Estimation for Ni sulfate.
[d] Calculated from lattice parameters.

3.2.7. Nickel macrocyclic compound

Some lipids in the archaeabacteria (Woese and Fox, 1977) have the structure of macrocyclic tetraether (Kushwaha et al., 1981). The isotopic fractionation of metals in macrocyclic compounds is hence of interest. Here, we estimate ln β of the Ni–DC18C6 complex in our chemical exchange experiment.

By using ln β (285 K) of $Ni(H_2O)_6^{2+}$, $NiCl(H_2O)_5^{+}$, and *trans*-$NiCl_2(H_2O)_4$, the relative abundance of these species at each HCl molarity, and the measured δ^{60}Ni fractionation between aqueous and organic phases, ln β of the Ni–DC18C6 complex was estimated. The analysis gives ln $\beta = 4.177‰$ (Table 6) at 285 K, which is equivalent with ln $\beta = 3.859‰$ at 298 K. In our experiment, the difference of ln β between the Ni–DC18C6 complex and other species (Ni^{2+}, $NiCl^{+}$, and $NiCl_2$) is measured as δ^{m}Ni. As shown in Table 6, the difference in ln β is in the order of $Ni^{2+} > NiCl^{+} > NiCl_2$. This suggests that the magnitude of δ^{m}Ni decreases by promoting the complexation of Ni^{2+} with Cl^{-}. Hence, it is natural that we observed smaller isotope fractionation at higher acidity as shown in Table 1.

3.2.8. Nickel carboxylate

The carboxyl group is a major functional group in humic acids (Schnitzer and Skinner, 1965) that control the reactions between cations and organic matters in groundwater. In seawater, it is known that reactions between amino acids, CO_2, and carbonates, can make soluble carbamino carboxylates (Neuberg et al., 1957). To enhance the knowledge on Ni isotope fractionation in reactions with organic ligands, we calculated ln β for nickel monooxalate, $NiC_2O_4(H_2O)_4$, dioxalate (bisoxalate), $Ni(C_2O_4)_2(H_2O)_2^{2-}$, and trioxalate (trisoxalate), $Ni(C_2O_4)_3^{4-}$, by the same quantum chemical calculations as described above. The molecular structures were computed based on published structural models (Krylov et al., 1976; Bickley et al., 1991). Only one *trans*-diaquabisoxalatenickel crystal structure, $Ni(C_2O_4)_2(H_2O)_2^{2-}$, is available in the literature for dipotassium bisoxalatonickel, $K_2[Ni(C_2O_4)_2(H_2O)_2]{\cdot}4H_2O$ (Román et al., 1993). The Ni–O bond lengths were reported to be 2.016 or 2.050 Å (C_2O_4) and 2.086 Å (H_2O). Our calculated Ni–O bond lengths are 2.038 Å (C_2O_4) and 2.224 Å (H_2O). The calculated Ni–O bond length is in good agreement with the crystal data for $C_2O_4^{2-}$. The intramolecular vibrations of $K_2[Ni(C_2O_4)_2(H_2O)_2]{\cdot}4H_2O$ was analyzed by Raman spectrometry (Bickley et al., 1991). Measurement of the symmetrical Ni–O ring stretch of $Ni(C_2O_4)_2^{2-}$ gave a value of 583 cm^{-1}, which is in good agreement with our calculation of 560 cm^{-1}. The calculated ln β values are reported in Table 6. Complexation with $C_2O_4^{2-}$ induces a decrease in ln β, i.e., $NiC_2O_4(H_2O)_4$ (6.348‰) > $Ni(C_2O_4)_2(H_2O)_2^{2-}$ (5.872‰) > $Ni(C_2O_4)_3^{4-}$ (4.275‰) at 298 K. ln β of Ni oxalates is larger than that of Ni–crown complex. This may be due to the stronger electron affinity of oxalate ions to Ni^{2+} (Watters and DeWitt, 1960) than that of oxygen donors of DC18C6.

3.3. Implications for Ni isotope systematics in the modern and ancient oceans

For all Ni species, the temperature dependence of ln β (Fig. 4) is estimated by using the relationship ln $\beta(T) = \ln \beta\ (298) \times (298/T)^2$ with the ln β values at 298 K compiled in Table 6. The variation of ln β among inorganic species at 298 K is 1.7‰ (Fig. 4a), while that among organic species at 298 K is 2.5‰ (Fig. 4b). It is clear that exchange reactions between simple inorganic and organic ligands can create isotope fractionation reaching ~2.5‰. This range encompasses the isotopic fractionation measured by Cameron et al. (2009) in methanogenic Archaea (δ^{60}Ni up to

1.46‰, i.e., ~0.73‰/amu). Therefore, our results suggest that abiotic fractionation of Ni in the ocean represents a major source of Ni isotopic variations and should be considered for the interpretation of Ni isotope data in modern and ancient sedimentary rocks.

To guide future work in Ni isotope systematics, we have calculated the speciation and the isotopic fractionation of Ni in the Archean and modern oceans (Fig. 5). Our calculations do not take into account the presence of organic ligands with strong affinities for Ni. We predict the isotopic composition of the main species of Ni in condition relevant the Archean ocean.

Ni species, i.e., $Ni(H_2O)_6^{2+}$, $NiOH(H_2O)_5^{+}$, $NiCl(H_2O)_5^{+}$, $NiSO_4(H_2O)_4$, $NiHCO_3(H_2O)_4^{+}$, and $NiCO_3(H_2O)_4$, are treated here. The chemical equilibrium reactions,

$$Ni^{2+} + H_2O \rightleftarrows NiOH^{+} + H^{+} \quad (13)$$

$$Ni^{2+} + SO_4^{2-} \rightleftarrows NiSO_4 \quad (14)$$

$$Ni^{2+} + HCO_3^{-} \rightleftarrows NiHCO_3^{+} \quad (15)$$

$$Ni^{2+} + CO_3^{2-} \rightleftarrows NiCO_3 \quad (16)$$

and reaction 1 for $NiCl^{+}$ are considered. For a seawater condition, [Ni(II)] ~10^{-8} M and pH ~8, higher order hydrolysis and polymerization (Baes and Mesmer, 1976; Hummel and Culti, 2003, and references therein), e.g., $Ni(OH)_3^{-}$, $Ni(OH)_4^{2-}$, Ni_2OH^{3-}, and $Ni_4(OH)_4^{4+}$, may be insignificant. Also higher order complexations of chloride and sulfate are not considered. Though there is a redox reaction between sulfide and sulfate ions as,

$$HS^{-} + 4H_2O \rightleftarrows SO_4^{2} + 9H^{+} + 8e^{-} \quad (17)$$

the standard redox potential of reaction 17 at pH 8.22 (a typical modern seawater condition, Macleod et al., 1994) is estimated to be −0.29 V in standard hydrogen electrode potential (Pourbaix, 1974). This is much smaller than Eh = 0.5 V for typical modern seawater (Macleod et al., 1979), and hence the formation of $NiSH^{+}$ is not considered.

To estimate the composition of Ni species and isotope fractionation between these, an appropriate combination of stability constants for reactions, 1 and 13–16 must be selected from literature data. Temperature of the modern ocean is around 291 K (global mean sea surface temperature), while that of the Archean has been reported to be up to 343 K (Robert and Chaussidon, 2006). Though the temperature difference affects the speciation and isotopic calculation, as a first approximation, we estimate them at a standard temperature, 298 K. The selected log K values are $\log K(NiCl^{+}) = 0.72$ (Turner et al., 1981), $\log K(NiOH^{+}) = -9.86$ (Turner et al., 1981), $\log K(NiSO_4) = 0.9$ (Byrne et al., 1988), $\log K(NiHCO_3^{+}) = 1.59$, and $\log K(NiCO_3) = 3.57$ (Smith and Martell, 1976). These constants were determined for ionic strength $I = 0.7$ M by using reported data (Zhorov et al., 1976). It should be noted that the $K(NiCl^{+})$ value used here is higher than that for HCl system (Bjerrum, 1988), while $K(NiSO_4)$ used here is smaller than the reported values obtained in laboratory experiments (Wasylkiewicz, 1990; Tsierkezos and Molinou, 2000; Chen et al., 2005, and references therein). The uncertainty of $K(NiHCO_3^{+})$ and $K(NiCO_3)$ is discussed in detail by Hummel and Culti (2003).

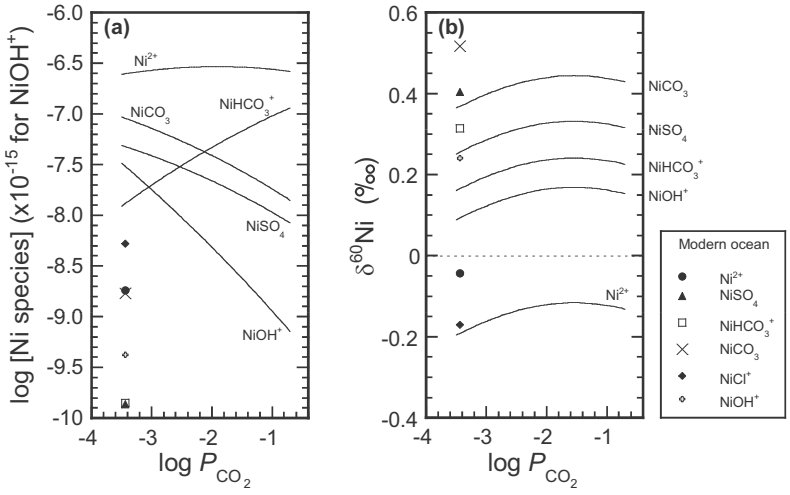

Fig. 5. Ni species in Modern and Archeans ocean and their isotopic fractionations as functions of partial pressure of CO_2. (a) Concentrations of Ni species in Archean and modern oceans. The curves show the estimated concentrations of Ni species in Archaean ocean. The marks show those in modern ocean. Total concentrations of Ni were set to be 400 nM for Archaean ocean and 9 nM for modern ocean (Konhauser et al., 2009). For modern ocean, pH, $[Cl^{-}]$, and $[HCO_3^{-}]$, reported by Macleod et al. (1994) were used. $[CO_3^{2-}]$ was calculated form an equation proposed by Walker (1983). Free $[SO_4^{-}]$ (Byrne et al., 1988) was used. For Archaean ocean, $[SO_4^{2-}]$, $[HCO_3^{-}]$, and $[CO_3^{2-}]$ were estimated from a literature (Walker, 1983). $[OH^{-}]$ was estimated from $[H^{+}]$ (Walker, 1983) and the ion product of water at 298 K, $-\log K_W = 13.995$ (Lide, 2008). Because of very low concentration, $[Cl^{-}]$ was not included in the estimation for Archaean ocean. The log K values of reactions 1, 13–17 (see text) were set to be 0.72, −9.86, 0.9, 1.59, and 3.57, respectively. Activity coefficients of all species were set to be unity as a diluted system. (b) Isotope fractionations of Ni species compared to the naturally occurring isotope ratios. $\delta^{60}Ni$ was estimated by using concentrations of Ni species shown in Fig. 5a and the ln β values at 298 K shown in Table 6. Curves show estimated $\delta^{60}Ni$ values of Ni species in Archaean ocean. Marks show those in modern ocean.

For the Archean ocean, the total concentration of Ni(II) was set to be 400 nM (Konhauser et al., 2009). Concentrations of H^+, SO_4^{2-}, HCO_3^-, and CO_3^{2-}, were read from Fig. 2 of Walker (1983). $[OH^-]$ was estimated from $[H^+]$ and the ion product of water at 298 K, $-\log K_W = 13.995$ (Lide, 2008). Because of a very low expected concentration (Walker, 1983), $[Cl^-]$ was not included in the speciation calculation.

For the modern ocean, the total concentration of Ni(II) was set to be 9 nM (Konhauser et al., 2009), and pH 8.22, $m(Cl^-) = 0.55$ mol/kg, and $m(HCO_3^-) = 0.0020$ mol/kg (Macleod et al., 1994) were used. $[OH^-]$ was estimated from pH and the ion product of water (Lide, 2008). $[CO_3^{2-}]$ was estimated using an equation given by Walker (1983) and $\log P(CO_2) \sim -3.44$ (read from a figure by Macleod et al., 1994). For sulfate, free ion concentration $m(SO_4^{2-}) = 0.0095$ mol/kg (Byrne et al., 1988) was used. Activity coefficients of all species were set to be unity as a diluted system. Hence, molal concentrations were used as well as molar concentrations, and stability constants were directly used without correction of ionic strength.

Concentrations of Ni species as functions of carbon dioxide partial pressure are plotted in Fig. 5a. For the modern ocean, our calculation results in mole fractions of Ni^{2+} (20%), $NiCl^+$ (57%), $NiCO_3$ (19%), $NiHCO_3^+$ (2%), and $NiSO_4$ (2%). Considering our simplified calculation, our results are in fairly good agreement with the results of Turner and Martino (2006). As an example for the condition of Archean ocean, at $\log P(CO_2) = -1$, the mole fractions of Ni species are: Ni^{2+} (68%), $NiCO_3$ (5%), $NiHCO_3^+$ (24%), and $NiSO_4$ (3%). This indicates that the major species of Ni(II) in the Archean ocean would be hydrated Ni^{2+} ion and Ni carbonates. Fig. 5b shows $\delta^{60}Ni$ for each Ni species. Heavier isotopes are fractionated in the order of $NiCO_3 > NiSO_4 > NiHCO_3^+ > NiOH^+$, whereas the inverse effect occurs in Ni^{2+} (and $NiCl^+$). This is the same order of $\ln \beta$ (Table 6). For example, $NiCO_3$ is enriched in heavy isotopes by ~0.6‰ compared to Ni^{2+}.

Experimentally and theoretically, we have demonstrated that ligand exchange reactions can create Ni isotope fractionation of ~1.25‰/amu (2.5‰ for the $^{60}Ni/^{58}Ni$ ratio). Therefore Ni isotope geochemistry might be used to trace the speciation of Ni in the ancient ocean.

4. CONCLUSION

In this study, we have investigated both theoretically and experimentally the isotopic fractionation of Ni at equilibrium between several species (hydrated Ni^{2+}, hydroxides, chlorides, sulfides, sulfate, and carbonates) and organic ligands (crown ether and oxalic acid). The isotopic effect of the distribution of Ni between ligands relevant to the modern and ancient ocean chemistry is ~1.25‰/amu (2.5‰ for the $^{60}Ni/^{58}Ni$ ratio), which is of the same magnitude as the isotopic fractionation created by methanogenic Archaea. Therefore, isotopic fractionation during the distribution of Ni between different species should not be neglected for the interpretation of the Ni isotopic record of sedimentary rocks.

ACKNOWLEDGMENTS

The authors thank the anonymous reviewers and the associate editor, Derek Vance, for their useful suggestions and constructive comments on the manuscript. T.F. thanks J. Garrecht Metzger for his help in improving the English of this paper. N.D. was supported by a Packard fellowship, the France Chicago Center, a Moore Distinguished Scholarship at the California Institute of Technology, NASA through grant NNX09AG59G, and NSF through grant EAR-0820807. F.M. was supported by NASA through grant NNX09AM64G.

REFERENCES

Abe M., Suzuki T., Fuji Y. and Hada M. (2008a) An *ab* initio study based on a finite nucleus model for isotope fractionation in the U(III)–(IV) exchange reaction system. *J. Chem. Phys.* **128**, 144309.

Abe M., Suzuki T., Fujii Y., Hada M. and Hirao K. (2008b) An *ab* initio molecular orbital study of the nuclear volume effects in uranium isotope fractionations. *J. Chem. Phys.* **129**, 164309.

Abe M., Suzuki T., Fujii Y., Hada M. and Hirao K. (2010) Ligand effect on uranium isotope fractionations caused by nuclear volume effects: an ab initio relativistic molecular orbital study. *J. Chem. Phys.* **133**, 044309.

Agulló-Rueda F., Calleja J. M., Martini M., Spinolo G. and Cariati F. (1987) Raman and infrared spectra of transition metal halide hexahydrates. *J. Raman Spectrosc.* **18**, 485–491.

Albarède F., Telouk P., Blichert-Toft J., Boyet M., Agranier A. and Nelson B. (2004) Precise and accurate isotopic measurements using multiple-collector ICPMS. *Geochim. Cosmochim. Acta* **68**, 2715–2744.

Al-Farawati R. and van den Berg C. M. G. (1999) Metal-sulfide complexation in seawater. *Mar. Chem.* **63**, 331–352.

Anbar A. D., Jarzecki A. A. and Spiro T. G. (2005) Theoretical investigation of iron isotope fractionation between $Fe(H_2O)_6^{3+}$ and $Fe(H_2O)_6^{2+}$: implications for iron stable isotope geochemistry. *Geochim. Cosmochim. Acta* **69**, 825–837.

Baes C. F. and Mesmer R. E. (1976) *The Hydrolysis of Cations*. Wiley, New York.

Baeyens B., Bradbury M. H. and Hummel W. (2003) Determination of aqueous nickel-carbonate and nickel-oxalate complexation constants. *J. Solut. Chem.* **32**, 319–339.

Balci N., Bullen T. D., Witte-Lien K., Sjanks W. C., Motelica M. and Mandernack K. W. (2006) Iron isotope fractionation during microbially stimulated Fe(II) oxidation and Fe(III) precipitation. *Geochim. Cosmochim. Acta* **70**, 622–639.

Beard B. L., Johnson C. M., Cox L., Sun H., Nealson K. H. and Aguilar C. (1999) Iron isotope biosignature. *Science* **285**, 1889–1892.

Bechtold D. B., Liu G., Dodgen H. W. and Hunt J. P. (1978) An oxygen-17 nuclear magnetic resonance study of the aquo nickel(II) sulfate system. *J. Phys. Chem.* **82**, 333–337.

Becke A. D. (1993) Density-functional thermochemistry: 3. The role of exact exchange. *J. Chem. Phys.* **98**, 5648–5652.

Bickley R. I., Edwards H. G. M. and Rose S. J. (1991) A Raman spectroscopic study of nickel(II) oxalate dihydrate, $NiC_2O_4{\cdot}2H_2O$, and dipotassium bisoxalatonickel(II) hexahydrate, $K_2Ni(C_2O_4)_2{\cdot}6H_2O$. *J. Mol. Struct.* **243**, 341–350.

Bickley R. I., Edwards H. G. M., Knowles A., Gustar R. E., Mihara D. and Rose S. J. (1993) Vibrational spectroscopic study of nickel(II) malonate, $Ni(COO{\cdot}CH_2{\cdot}COO){\cdot}2H_2O$ and its aqueous solution. *J. Mol. Struct.* **296**, 21–28.

Bigeleisen J. and Mayer M. G. (1947) Calculation of equilibrium constants for isotopic exchange reactions. *J. Chem. Phys.* **15**, 261–267.

Bigeleisen J. (1996) Nuclear size and shape effects in chemical reactions: isotope chemistry of the heavy elements. *J. Am. Chem. Soc.* **118**, 3676–3680.

Bjerrum J. (1988) Estimation of small stability constants in aqueous solution. The nickel(II)-chloride system. *Acta Chem. Scand. A* **42**, 714–716.

Bock C. W., Markham G. D., Katz A. K. and Glusker J. P. (2006) The arrangement of first- and second-shell water molecules around metal ions. Effects of charge and size. *Theor. Chem. Accounts* **115**, 100–112.

Bruland K. W. (1980) Oceanographic distributions of cadmium, zinc, nickel, and copper in the North Pacific. *Earth Planet. Sci. Lett.* **47**, 176–198.

Bruland K. W. and Lohan M. C. (2003) The control of trace metals in seawater. In *Treatise on Geochemistry* (eds. H. D. Holland and K. K. Turekian). Elsevier, Oxford.

Byrne R. H., Kump L. R. and Cantrell K. J. (1988) The influence of temperature and pH on trace metal speciation in seawater. *Mar. Chem.* **25**, 163–181.

Cameron V., Vance D., Archer C. and House C. (2009) A biomarker based on the stable isotopes of nickel. *Proc. Natl. Acad. Sci. USA* **27**, 10944–10948.

Caminiti R., Licheri G., Piccaluga G. and Pinna G. (1977) X-ray-diffraction and structure of $NiCl_2$ aqueous solutions. *Faraday Discuss.* **64**, 62–68.

Caminiti R. (1982) An X-ray diffraction study on SO_4^{2-}–H_2O interactions in the presence of nickel and magnesium ions. *Chem. Phys. Lett.* **88**, 103–108.

Caminiti R. (1986) On nickel-sulfate contacts and $SO_4^{=}$–H_2O interactions in aqueous solutions. *J. Chem. Phys.* **84**, 3336–3338.

Chen T., Hefter G. and Buchner R. (2005) Ion association and hydration in aqueous solutions of nickel(II) and cobalt(II) sulfate. *J. Solut. Chem.* **34**, 1045–1066.

Cook D. L., Wadhwa M., Clayton R. N., Dauphas N., Janney P. E. and Davis A. M. (2007) Mass-dependent fractionation of nickel isotopes in meteoritic metal. *Meteor. Planet. Sci.* **42**, 2067–2077.

Crosby H. A., Johnson C. M., Roden E. E. and Beard B. L. (2005) Coupled Fe(II)–Fe(III) electron and atom exchange as a mechanism for Fe isotopic fractionation during dissimilatory iron oxide reduction. *Environ. Sci. Technol.* **39**, 6698–6704.

Croal L. R., Johnson C. M., Beard B. L. and Newman D. K. (2004) Iron isotope fractionation by Fe(II)-oxidizing photoautotrophic bacteria. *Geochim. Cosmochim. Acta* **68**, 1227–1242.

Dauphas N. and Rouxel O. (2006) Mass spectrometry and natural variations of iron isotopes. *Mass Spectrom. Rev.* **25**, 515–550.

Dauphas N., Cook D. L., Sacarabany A., Fröhlich C., Davis A. M., Wadhwa M., Pourmand A., Rauscher T. and Gallino R. (2008) Iron 60 evidence for early injection and efficient mixing of stellar debris in the protosolar nebula. *Astrophys. J.* **686**, 560–569.

Dimaras P. I. (1957) Morphology and structure of anhydrous nickel sulphate. *Acta Crystallogr.* **10**, 313–315.

Domagal-Goldman S. D., Paul K. W., Sparks D. L. and Kubicki J. D. (2008) Quantum chemical study of the Fe(III)-desferrioxamine B siderophore complex-Electronic structure, vibrational frequencies, and equilibrium Fe-isotope fractionation. *Geochim. Cosmochim. Acta* **73**, 1–12.

Donat J. R., Lao K. and Bruland K. W. (1994) Speciation of dissolved copper and nickel in South San Francisco Bay: a multi-method approach. *Anal. Chim. Acta* **284**, 547–571.

Dupont C. L., Barbeau K. and Palenik B. (2008) Ni uptake and limitation in marine synechococcus strains. *Appl. Environ. Microbiol.* **74**, 23–31.

Edwards H. G. M. and Knowles A. (1992) Vibrational spectroscopic study of nickel (II) formate, $Ni(HCO_2)_2$, and its aqueous solution. *J. Mol. Struct.* **268**, 13–22.

Escuer A., Vicente R., Kumar S. B., Solans X., Font-Bardía M. and Caneschi A. (1996) A novel pentadentate coordination mode for the carbonato bridge: synthesis, crystal structure, and magnetic behavior of $(\mu_3\text{-}CO_3)[Ni_3(Medpt)_3(NCS)_4]$, a new trinuclear nickel(II) carbonato-bridged complex with strong antiferromagnetic coupling. *Inorg. Chem.* **35**, 3094–3098.

Fricke G. and Heilig K. (2004) *Nuclear Charge Radii (Landolt-Bornstein Numerical Data and Functional Relationships in Science and Technology-New Series)* (ed. Schopper H.) Springer, Berlin.

Frisch M. J., Trucks G. W., Schlegel H. B., Scuseria G. E., Robb M. A., Cheeseman J. R., Montgomery Jr., J. A., Vreven T., Kudin K. N., Burant J. C., Millam J. M., Iyengar S. S., Tomasi J., Barone V., Mennucci B., Cossi M., Scalmani G., Rega N., Petersson G. A., Nakatsuji H., Hada M., Ehara M., Toyota K., Fukuda R., Hasegawa J., Ishida M., Nakajima T., Honda Y., Kitao O., Nakai H., Klene M., Li X., Knox J. E., Hratchian H. P., Cross J. B., Adamo C., Jaramillo J., Gomperts R., Stratmann R. E., Yazyev O., Austin A. J., Cammi R., Pomelli C., Ochterski J. W., Ayala P. Y., Morokuma K., Voth G. A., Salvador P., Dannenberg J. J., Zakrzewski V. G., Dapprich S., Daniels A. D., Strain M. C., Farkas O., Malick D. K., Rabuck A. D., Raghavachari K., Foresman J. B., Ortiz J. V., Cui Q., Baboul A. G., Clifford S., Cioslowski J., Stefanov B. B., Liu G., Liashenko A., Piskorz P., Komaromi I., Martin R. L., Fox D. J., Keith T., Al-Laham M. A., Peng C. Y., Nanayakkara A., Challacombe M., Gill P. M. W., Johnson B., Chen W., Wong M. W., Gonzalez C. and Pople J. A. (2003) *Gaussian 03, Revision B.05*, Gaussian, Inc., Pittsburgh PA.

Fujii T., Moynier F. and Albarède F. (2009a) The nuclear field shift effect in chemical exchange reactions. *Chem. Geol.* **267**, 139–156.

Fujii T., Moynier F., Telouk P. and Albarède F. (2009b) Nuclear field shift effect in the isotope exchange reaction of cadmium using a crown ether. *Chem. Geol.* **267**, 157–163.

Fujii T., Moynier F., Uehara A., Abe M., Yin Q.-Z., Nagai T. and Yamana H. (2009c) Mass-dependent and mass-independent isotope effects of zinc in a redox reaction. *J. Phys. Chem. A* **113**, 12225–12232.

Fujii T., Moynier F., Telouk P. and Abe M. (2010) Experimental and theoretical investigation of isotope fractionation of zinc between aqua, chloro, and macrocyclic complexes. *J. Phys. Chem. A* **114**, 2543–2552.

Gramlich J. W., Machlan L. A., Barnes I. L. and Paulsen P. J. (1989) Absolute isotopic abundance ratios and atomic weight of a reference sample of nickel. *J. Res. Natl. Inst. Stand. Technol.* **94**, 347–356.

Hill P. S., Schauble E. A., Shahar A., Tonui E. and Young E. D. (2009) Experimental studies of equilibrium iron isotope fractionation in ferric aquo–chloro complexes. *Geochim. Cosmochim. Acta* **73**, 2366–2381.

Hummel W. and Culti E. (2003) Nickel aqueous speciation and solubility at ambient conditions: a thermodynamic elegy. *Mon. Chem.* **134**, 941–973.

Jepson B. E. and Cairns G. A. (1979) Lithium isotope effects in chemical exchange with (2,2,1) cryptand, *MLM-2622*.

Johnson C. M., Beard B. L. and Roden E. E. (2008) The iron isotope fingerprints of redox and biogeochemical cycling in the

modern and ancient Earth. *Annu. Rev. Earth Planet. Sci.* **36**, 457–493.

Jönsson P., He X., Fischer C. F. and Grant I. P. (2007) The grasp2K relativistic atomic structure package. *Comput. Phys. Commun.* **177**, 597–622.

King W. H. (1984) *Isotope Shifts in Atomic Spectra*. Plenum Press, New York.

Kleinberg R. (1969) Crystal structure of $NiCl_2{\cdot}6H_2O$ at room temperature and 4.2 K by neutron diffraction. *J. Chem. Phys.* **50**, 4690–4696.

Konhauser K. O., Pecoits E., Lalonde S. V., Papineau D., Nisbet E. G., Barley M. E., Arndt N. T., Zahnle K. and Kamber B. S. (2009) Oceanic nickel depletion and a methanogen famine before the Great Oxidation Event. *Nature* **458**, 750–753.

Krylov E. I., Makurin Yu. N. and Kasimov G. G. (1976) Electronic structure of nickel oxalate. *J. Struct. Chem.* **17**, 347–350.

Kushwaha S. C., Tates M., Sprott G. D. and Smith I. C. P. (1981) Novel polar lipids from the methanogen *methanospirillum hungatei* GP1. *Biochim. Biophys. Acta* **664**, 156–173.

Lee C. T., Yang W. T. and Parr R. G. (1988) Development of the colle-salvetti correlation-energy formula into a functional of the electron-density. *Phys. Rev. B* **37**, 785–789.

Li J., Fisher C. L., Chen J. L., Bashford D. and Noodleman L. (1996) Calculation of redox potentials and pK_a values of hydrated transition metal cations by a combined density functional and continuum dielectric theory. *Inorg. Chem.* **35**, 4694–4702.

Licheri G., Paschina G., Piccaluga G. and Pinna G. (1984) X-ray diffraction study of aqueous solutions of $NiSO_4$ and $MnSO_4$. *J. Chem. Phys.* **81**, 6059–6063.

Licheri G., Paschina G., Piccaluga G. and Pinna G. (1986) Comment on: "Nickel-sulfate contacts and $SO_4^{=}$–H_2O interactions in aqueous solutions". *J. Chem. Phys.* **85**, 3135.

Lide D. R. (2008) *CRC Handbook of Chemistry and Physics*, 89th ed. CRC Press, Boca Raton.

Macleod G., Mcneown C., Hall A. J. and Russel M. J. (1994) Hydrothermal and oceanic pH conditions of possible relevance to the origin of life. *Orig. Life Evol. Biosph.* **24**, 19–41.

Magini M. (1979) Solute structuring in aqueous iron(III) sulphate solutions: evidence for the formation of iron(III)–sulphate complexes. *J. Chem. Phys.* **70**, 317–324.

Magini M. (1981) Hydration and complex formation study on concentrated solutions [M = Co(II), Ni(II), Cu(II)] by X-ray diffraction technique. *J. Chem. Phys.* **74**, 2523–2529.

Magini M., Paschina G. and Piccaluga G. (1982) Ni–Cl bonding in concentrated Ni(II) aqueous solutions at high Cl^-/Ni^{2+} ratios. An X-ray diffraction investigation. *J. Chem. Phys.* **76**, 1116–1121.

Mandernack K. W., Bazylinski D. A., Shanks W. C. and Bullen T. D. (1999) Oxygen and iron isotope studies of magnetite produced by magnetitactic bacteria. *Science* **285**, 1892–1896.

Marcus Y. (1985) *Ion Solvation*. John Wiley & Sons, New York.

Mizuno J. (1961) Crystal structure of nickel chloride hexahydrate, $NiCl_2{\cdot}6H_2O$. *J. Phys. Soc. Jpn.* **16**, 1574–1580.

Moynier F., Blichert-Toft J., Telouk P., Luck J. M. and Albarede F. (2007) Comparative stable isotope geochemistry of Ni, Cu, Zn, and Fe in chondrites and iron meteorites. *Geochim. Cosmochim. Acta* **71**, 4365–4379.

Neilson G. W. and Enderby J. E. (1978) Hydration of Ni^{2+} in aqueous solutions. *J. Phys. C Solid State Phys.* **11**, L625–L628.

Neuberg C., Grauer A., Kreidl M. and Lowy H. (1957) The role of the carbamate reaction in the calcium and phosphorus cycles in nature. *Arch. Biochem. Biophys.* **70**, 70–79.

Nishizawa K., Ishino S., Watanabe H. and Shinagawa M. (1984) Lithium isotope separation by liquid–liquid extraction using benzo-15-crown-5. *J. Nucl. Sci. Technol.* **21**, 694–701.

Nishizawa K., Miki T., Ikeda R., Fujii T., Yamamoto T. and Nomura M. (1997) Isotopic enrichment of nickel in aqueous solution/crown ether system. *J. Mass Spectrom. Soc. Jpn.* **45**, 521–527.

Nomura M., Higuchi N. and Fujii Y. (1996) Mass dependence of uranium isotope effects in the U(IV)–U(VI) exchange reaction. *J. Am. Chem. Soc.* **118**, 9127–9130.

O'Connor B. H. and Dale D. H. (1966) A neutron diffraction analysis of the crystal structure of tetragonal nickel sulphate hexadeuterate. *Acta Crystallogr.* **21**, 705–709.

Pattanaik S., Huggins F. E., Huffman G. P., Linak W. P. and Miller C. A. (2007) XAFS studies of nickel sulfur speciation in residual oil fly-ash particulate matters (ROFA PM). *Environ. Sci. Technol.* **41**, 1104–1110.

Pourbaix M. (1974) *Atlas of Electrochemical Equilibria in Aqueous Solutions*. NACE, Hiuston.

Price N. M. and Morel F. M. M. (1991) Colimitation of phytoplankton growth by nickel and nitrogen. *Limnol. Oceanogr.* **36**, 1071–1077.

Ptasiewicz-Bak H., Olovsson I. and McIntyre G. J. (1997) Charge density in orthorhombic $NiSO_4{\cdot}7H_2O$ at room temperature and 25 K. *Acta Crystallogr. B* **53**, 325–336.

Ptasiewicz-Bak H., Olovsson I. and McIntyre G. J. (1999) Charge density in $NiCl_2{\cdot}4H_2O$ at 295 and 30 K. *Acta Crystallogr. B* **55**, 830–840.

Pye C. C., Corbeil C. R. and Rudolph W. W. (2006) An *ab initio* investigation of zinc chloro complexes. *Phys. Chem. Chem. Phys.* **8**, 5428–5436.

Rickard D. and Luther, III, G. W. (2006) Metal sulfide complexes and clusters. *Rev. Miner. Geochem.* **61**, 421–504.

Robert F. and Chaussidon M. (2006) A palaeotemperature curve for the Precambrian oceans based on silicon isotopes in cherts. *Nature* **443**, 969–972.

Rosseinsky D. R. (1965) Electrode potentials and hydration energies. Theories and correlations. *Chem. Rev.* **65**, 467–490.

Román P., Guzmán-Miralles C. and Luque A. (1993) Structure of dipotassium *trans*-diaquabis(oxalate-*O*,*O*′)nickelate(II)-water (1/4). *Acta Cryst.* **C49**, 1336–1339.

Rudolph W. W. and Pye C. C. (1999) Zinc(II) hydration in aqueous solution. A Raman spectroscopic investigation and an *ab-initio* molecular orbital study. *Phys. Chem. Chem. Phys.* **1**, 4583–4593.

Rulíšek L. and Havlas Z. (1999) Ab initio calculations of monosubstituted (CH_3OH, CH_3SH, NH_3) hydrated ions of Zn^{2+} and Ni^{2+}. *J. Phys. Chem. A* **103**, 1634–1639.

Russell W. A., Papanastassiou D. A., Tombrello T. A. and Epstein S. (1977) Search for Ca isotopic fractionation and correlation of Ca and O effects. *Lunar Sci.* **8**, 823–825.

Russell W. A., Papanastassiou D. A. and Tombrello T. A. (1978) Ca isotope fractionation on earth and other solar-system materials. *Geochim. Cosmochim. Acta* **42**, 1075–1090.

Saito M. A., Sigman D. M. and Morel F. M. M. (2003) The bioinorganic chemistry of the ancient ocean: the co-evolution of cyanobacterial metal requirements and biogeochemical cycles at the Archean-Proterozoic boundary? *Geochim. Cosmochim. Acta* **356**, 308–318.

Saito M. A., Moffett J. W. and DiTullio G. R. (2004) Cobalt and nickel in the Peru upwelling region: a major flux of labile cobalt utilized as a micronutrient. *Global Biogeochem. Cycles* **18**, GB4030.

Sandstrom D. R. (1979) Ni^{2+} coordination in aqueous $NiCl_2$ solutions: study of the extended X-ray absorption fine structure. *J. Chem. Phys.* **71**, 2381–2386.

Schauble E. A. (2007) Role of nuclear volume in driving equilibrium stable isotope fractionation of mercury, thallium, and other very heavy elements. *Geochim. Cosmochim. Acta* **71**, 2170–2189.

Schnitzer M. and Skinner S. I. M. (1965) Organo-metallic interactions in soils: 4. Carboxyl and hydroxyl groups in organic matter and metal retention. *Soil Sci.* **99**, 278–284.

Sclater F. R., Boyle E. and Edmond J. M. (1976) On the marine geochemistry of nickel. *Earth Planet. Sci. Lett.* **31**, 119–128.

Smith D. W. (1977) Ionic hydration enthalpies. *J. Chem. Educ.* **54**, 540–542.

Smith R. M. and Martell A. E. (1976). .

Thauer R. K. (1998) Biochemistry of methanogenesis: a tribute to Marjory Stephenson. *Microbiology* **144**, 2377–2406.

Tsierkezos N. G. and Molinou I. E. (2000) Limiting molar conductances and thermodynamic association constants for nickel(II), cadmium(II), magnesium(II), and copper(II) sulfates in mixtures of methanol and water at 293.15 K. *J. Chem. Eng. Data* **45**, 819–822.

Turner D. R., Whitfield M. and Dickson A. G. (1981) The equilibrium speciation of dissolved components in freshwater and sea water at 25 °C and 1 atm pressure. *Geochim. Cosmochim. Acta* **45**, 855–881.

Turner A. and Martino M. (2006) Modelling the equilibrium speciation of nickel in the Tweed Estuary, UK: voltametric determination and simulations using WHAM. *Mar. Chem.* **102**, 198–207.

Urey H. C. (1947) The thermodynamic properties of isotopic substances. *J. Chem. Soc.*, 562–581.

Vraspir J. M. and Butler A. (2009) Chemistry of marine ligands and siderophores. *Annu. Rev. Mar. Sci.* **1**, 43–63.

Waizumi K., Ohtaki H., Masuda H., Fukushima N. and Watanabe Y. (1992a) Density functional calculations on the geometries and dissociation energies of $[M(H_2O)_6]^{2+}$ ions. $M^{2+} = Cr^{2+}$, Mn^{2+}, Fe^{2+}, Co^{2+}, Ni^{2+}, Cu^{2+}, and Zn^{2+}. *Chem. Lett.*, 1489–1492.

Waizumi K., Masuda H. and Ohtaki H. (1992b) X-ray structural studies of $FeBr_2{\cdot}4H_2O$, $CoBr_2{\cdot}4H_2O$, $NiCl_2{\cdot}4H_2O$ and $CuBr_2{\cdot}4H_2O$. *cis*/*trans* Selectivity in transition metal(II) dihalide tetrahydrate. *Inorg. Chim. Acta* **192**, 173–181.

Waizumi K., Kouda T., Tanio A., Fukushima N. and Ohtaki H. (1999) Structural studies on saturated aqueous solutions of manganese(II), cobalt(II), and nickel(II) chlorides by X-ray diffraction. *J. Solut. Chem.* **28**, 83–100.

Walker J. C. G. (1983) Possible limits on the composition of the Archaean ocean. *Nature* **302**, 518–520.

Wasylkiewicz S. (1990) Ion association in aqueous solutions of electrolytes: II. Mathematical model for sulphates of bivalent metals. *Fluid Phase Equilibria* **57**, 277–296.

Watters J. I. and DeWitt R. (1960) The complexes of nickel(II) ion in aqueous solutions containing oxalate ion and ethylenediamine. *J. Am. Chem. Soc.* **82**, 1333–1339.

Wikstrom J. P., Filatov A. S., Mikhalyova E. A., Shatruk M., Foxmane B. M. and Rybak-Akimova E. V. (2010) Carbonate formation within a nickel dimer: synthesis of a coordinatively unsaturated bis(μ-hydroxo) dinickel complex and its reactivity toward carbon dioxide. *Dalton Trans.* **39**, 2504–2514.

Woese C. R. and Fox G. E. (1977) Phylogenetic structure of the prokaryotic domain: the primary kingdoms. *Proc. Natl. Acad. Sci. USA* **74**, 5088–5090.

Zhorov V. A., Bezborodova A. and Popov N. I. (1976) Predominance area diagrams and equilibrium ratios of inorganic form of Co and Ni in oceanic water. *Oceanology* **16**, 463.

Associate editor: Derek Vance